The Role of SO-group-based Additives in Improving the Rechargeable Aluminium-air Batteries

Soraya Hosseini[1], Zhe-Yu Liu[1], Chen-Tzu Chuan[1], Salman M. Soltani [2], L.V.Venkata Krishna[1,3], Yuan-Yao Li[1,4,*]

[1]Department of Chemical Engineering, National Chung Cheng University, Min-Hsiung, Chiayi 62102, Taiwan

[2]Department of Chemical Engineering, Brunel University London, Uxbridge UB8 3PH, United Kingdom

[3]Department of Mechanical Engineering, National Chung Cheng University, Min-Hsiung, Chiayi 62102, Taiwan

[4]Advanced Institute of Manufacturing with High-Tech Innovations, National Chung Cheng University, Chia-Yi 62102, Taiwan.

* Corresponding author's E-mail address: chmyyl@ccu.edu.tw

* Corresponding author's Tel: 886-5-2920411

Abstract

The influence of various sulphur-oxygen (SO) group additives has been investigated in retarding the self-corrosion of Al anode in a 4M KOH solution, in order to effectively enhance the overall performance. The studied additives in this work were all found to be capable of decreasing H_2 evolution, and could mitigate aluminium self-corrosion, with the corrosion inhibition towards the cathodic protection process. The less pitting corrosion and holes were observed for inorganic additives in comparison to the organic counterparts. The Al-air batteries demonstrated an improvement in the discharge capacities: 2604, 2393, 2348 and 2048 $mAhg^{-1}$ for Na_2SO_4, Na_2SO_3, C_2H_6SO, and $C_6H_5SO_2OH$, respectively, in comparison to that associated with the 4M KOH (2021 $mAhg^{-1}$). $K_2S_2O_8$, an inorganic additive, exhibited a hydrogen evolution efficiency of 21%, but the lowest discharge performance (1973 $mAhg^{-1}$). This may be due to the instability of the anions in redox reactions. The low inhibition efficiency of the hybrid additives in Al self-corrosion, when compared to single additives, may be ascribed to the involvement of Al^{3+} in complex formation of the inorganic-organic hybrid additives. A stable discharge-charge cycling test over 6 h with a voltage gap of around 0.7 V is observed for Na_2SO_4, demonstrating the efficient performance compared to the additive-free KOH electrolyte. It could be concluded that efficient additives containing SO group, successfully mitigated the self-corrosion and hydrogen evolution associated with the Al anode that was confirmed with DFT results.

Keywords: Rechargeable aluminium-air battery; Electrolyte additives; Inorganic salts; Organic solvent; Hydrogen evolution reaction

1. Introduction:

The scarcity and cost of lithium resources set more attentions towards probing into other metals as alternatives for Li-based batteries. Zinc, aluminium, sodium, magnesium, as more abundant metals, could serve as such alternatives. Since aluminium, the 13th abundant element in the earth's crust with a high energy density, has several advantages and prospects over other metals [1], Al-based batteries are regarded as promising substitutes. Al-batteries have a high theoretical specific capacity (2980 $mAhg^{-1}$) and a low toxicity; are safe and inexpensive [2]. However, several inherent drawbacks, namely, tendency for self-corrosion and hydrogen gas evolution in alkaline medium under both open-circuit and discharge conditions, hinder their commercialization. The inferior positive movement of corrosion potential leads to a reduction in Al utilisation. Furthermore, the deposition of by-products (i.e. $Al(OH)_3$, and Al_2O_3) on the electrode's surface suppresses electrochemical reactions [3-5].

Recent developments based on modifying electrolytes, anodes (Al) and the catalytic activity of cathodes are turned up to ameliorate batteries' performance. The effect of alloy elements with high hydrogen overpotentials (e.g. Zn, Mg, Sn, Mn, Pb and Bi) has revealed significant repression of self-corrosion and H_2 valuation [6-8]. However, the fabrication process is fairly expensive compared with other techniques. Numerous research have been conducted to modify the catalyst's efficiency in oxygen reduction reaction (ORR) and oxygen evolution reduction (OER) via the employment of bi-functional catalysts, metal-nitrogen carbon (M-N-C), metal-organic frameworks (MOF) and free-metal catalysts. This is due to the fact that the commercialization of Al-air batteries requires efficient yet economical catalysts which can also demonstrate faster oxygen reduction reactions [9-11].

Electrolyte additives have also been extensively employed by many researchers to enhance the performance of Al-air batteries. Apparently, additives are competent at reducing the rate of undesired reactions, increasing anode utilisation, enhancing the discharge capacity and the cycle life of batteries. Additives including inorganics [12,13], organics [14,15], polymers [16], ionic liquids [17,18], concentrated salts [19] and hybrid electrolytes [20,21] are known to be effective in Al-air batteries. Additives may act in different ways; for instance, the may generated a protective film on the anode electrode and form a complex with undesired products in order to prevent the precipitation of $Al(OH)_3$ or Al_2O_3 over electrodes. Alongside, providing a porous and

uniform layer may accelerate ion transport through the electrolyte/electrode and may enhance the dissolution of $Al_2O_3/Al(OH)_3$ species [22]. It was reported that a sedimentary layer is usually formed on Al's surface upon the addition of inorganic additives [23]. Organic additives containing polar groups (i.e. N, O, P and S) may bind through heteroatoms, containing lone pair of electrons, onto the Al's surface. This may result in the formation of a barrier layer to prevent the initiation of the self-corrosion process [24,25]. Due to the interaction mechanism between the functional groups of organic additives and the Al's surface, organic additives with high molecular weights and large polar groups are suggested for to slow down the corrosion processes. In addition, the use of hybrid additives has been also reported. However, satisfactory inhibition was not observed. Therefore, new strategies for hybrids of inorganic/organic additives are require to be looked into, in order to achieve a better suppressive effect compared to single additives [1, 2, 20-22, 26, 27].

Alkaline electrolytes with high conductivity could eliminate the aluminium oxide on the surface of Al metal and refine the electrochemical performance. However, serious self-corrosion of Al anode and hydrogen evolution reaction may be observed with the employment of alkaline solutions. Non-aqueous ionic liquids and solid-state electrolytes allow for a lower corrosion rate compared to alkaline aqueous electrolytes; however, low ionic conductivity, low solubilities of discharging products, volatility and flammability have limited their utilisation in Al-air batteries [28]. Therefore, modification of electrolytes with efficient additives is highly required to resolve the mentioned issues in order to pave the way for large-scale deployment of Al batteries.

In this work, different SO-containing chemicals i.e. $K_2S_2O_8$, Na_2SO_4, Na_2SO_3, $C_6H_5SO_2OH$ and C_2H_6SO have been used as additives to investigate self-corrosion and H_2 evolution reaction over Al anode electrode. H_2 evolution reaction test was carried out to determine their efficiencies in reducing the self-corrosion of Al anode. The corrosion suppression behaviour and the discharge performance of Al anode was further scrutinized in electrolytes containing SO groups, in Al-air batteries. Subsequently, electrochemical window, open circuit potential, chronoamperometry, potentiodynamic polarization and electrochemical impedance spectroscopy experiments were carried out to study the electrochemical behaviour of the Al anode in alkaline/additive electrolyte. Scanning electron microscopy (SEM), X-ray diffraction spectroscopy (XRD), X- ray photoelectron spectroscopy and contact angle measurement were employed to examine the surface morphology and the composition of the aluminium anode after the corrosion process. The air (cathode) catalyst was fabricated based on metal-organic framework (Co_3O_4/NC-CNT) in an in-house made cell used in our earlier study [29]. The feasibility

of rechargeable Al-air battery and discharge performance were evaluated using inorganic and organic additives.

2. Experimental Procedures

2.1 Materials

Potassium hydroxide (KOH pellet, 85%) was purchased from Honeywell Fluka and used in the preparation of the electrolyte solution (4M KOH). Inorganic and organic additives (i.e. $K_2S_2O_8$, Na_2SO_4, Na_2SO_3, $C_6H_5SO_2OH$ and C_2H_6SO - of analytical grade) were employed as additives. Inorganic metal salts $Co(NO_3)_2 \cdot 6H_2O$ (98%, Alfa), $Zn(NO_3)_2 \cdot 6H_2O$ (99%, Alfa), Carbon C65 (Timical Super C65), 2-methylimidazole ($C_4H_6N_2$, 99%, Sigma), PTFE (30 wt.% in solution) were used in the preparation of the air cathode. Commercial-grade pure aluminium (>99%) was used as the anode electrode. Nickel mesh (diamond hole, 99.99%) was used as current collector.

2.2 Electrochemical Measurements

The electrochemical tests were carried out using a three-electrode cell comprising Ag/AgCl as reference electrode, platinum foil as counter electrode, and an aluminium working electrode, using CHI electrochemical workstation (680C & 7081D) and ZAHNER scientific instruments. All measurements were carried out after a 15-minute immersion of aluminium in the electrolyte in order to stabilize the corrosion potential. The open circuit potential (OCP) was performed for 6000 s. The electrochemical window was recorded using two platinum foils as counter and the working electrodes in the potential range between -2 and 2 V. The potentiodynamic polarization was performed in the region of -1.0 to -1.7 V at a scan rate of 0.05 Vs^{-1}. The electrochemical impedance spectroscopy (EIS) experiments were executed in a frequency range between 1 MHz and 1 Hz at a sinusoidal potential perturbation of 5 mV in amplitude. Ec-lab software was employed to obtain the equivalent circuit model for fitting the EIS data.

An in-house battery was assembled to investigate the inhibitive effects of the applied additives. In preparation of air cathode catalyst, zeolitic imidazolate framework compound (ZIF67/ZIF8) was prepared following the steps taken in our earlier work [29]. The prepared ZIF67/ZIF8 was carbonized at 800 ºC under N_2 gas flow for 5 h, which was then used as the catalyst for the air cathode. Three-layer structure, including a current collector (Nickel mesh), a catalytic layer (carbonized ZIF67@ZIF8 /Carbon C65/ binder), and a gas diffusion layer GDL (carbon C65/ binder), was fabricated and served as the air cathode. The carbonized ZIF67@ZIF8 paste was manufactured in

sheets by using a rolling machine, which was coated over one side of the nickel mesh as the catalytic layer. The prepared (microporous) GDL sheet layer was coated on the other side of the nickel mesh. Finally, the three layers were kept pressed under 50 MPa for 5 min to obtain the air cathode layer. A 0.5 mm think aluminium sheet was used as the anode electrode. 4M KOH, with and without additives, was used as the electrolyte. The galvanostatic discharge capacities of the cells, at a current density of 10 $mAcm^{-2}$ with different electrolytes, were examined using a NEWARE battery tester. Furthermore, the galvanostatic discharge/charge test was performed for a discharge step of 10 min and a charge step of 20 min at a current density of 10 $mAcm^{-2}$.

2.3 Hydrogen Evaluation Test

Hydrogen generation rate is estimated by a simple setup including a glass vacuum bottle, a plastic syringe and connection tubes as shown in Figure S1. The 4M KOH solution with different additives was used as the electrolyte. 10 ml of the electrolyte (containing additives and KOH) together with the aluminium plate (0.33 cm^2) were placed in the glass vacuum bottle. The rate of Al corrosion was determined after complete dissolution of Al and subsequently, measuring the volume of the released hydrogen (as a consequence of the self-corrosion of Al). The hydrogen evolution rate (R) and the inhibition efficiency (η) are expressed using the given equations [30]:

$$R_{H2} = \frac{V_{H2}}{S \times t} \quad (1)$$

$$\eta = \frac{R_o - R_{inh}}{R_o} \times 100 \quad (2)$$

where, V_{H2}, t and S stand for the volume of hydrogen gas produced, the immersion time, and the surface area of the aluminium sample, respectively. Similarly, R_o and R_{inh} are the hydrogen evolution rate in the KOH and the KOH/additive solutions, respectively.

3. Results and Discussion

3.1 Electrochemical Characterization

Table 1 shows the hydrogen evolution rate along with the inhibition efficiencies of the Al anode in different types of electrolytes, with and without additive. The hydrogen evolution rate reaches 0.888 ml $cm^{-2}min^{-1}$ when using the additive-free electrolyte (4M KOH), while the lower amount of H_2 gas released was observed with KOH in the presence of the additives. The electrolytes containing the additives show the inhibition efficiencies of 21, 35, 29, 43 and 42 ml $cm^{-2}min^{-1}$, corresponding to $K_2S_2O_8$, Na_2SO_4,

Na_2SO_3, $C_6H_5SO_2OH$ and C_2H_6SO additives, respectively. The results indicate that all the additives can inhibit the self- corrosion of the Al's surface in the 4M KOH electrolyte. The highest inhibition efficiency is around 43% with usage of 10 v/v% 1M $C_6H_5SO_2OH$/KOH as the electrolyte. The inhibition efficiencies of the additives decrease in the order of: $C_6H_5SO_2OH > C_2H_6SO > Na_2SO_4 > Na_2SO_3 > K_2S_2O_8 >$ KOH. The high protection efficiency of organic additives may be attributed to larger functional groups integrated with the SO groups for a better protection of Al's surface - inhibiting self-corrosion and H_2 evaluation more effectively than the inorganic additives.

Table 1: Hydrogen evolution rates of various inhibitors in the 4M KOH electrolyte.

Electrolyte	Evolution rate ml $cm^{-2}min^{-1}$	Inhibition efficiency %
KOH	0.88	_
10%v/v 1M $K_2S_2O_8$	0.70	21
10%v/v 1MNa_2SO_4	0.58	35
10%v/v 1M Na_2SO3	0.63	29
10%v/v 1M $C_6H_5SO_2OH$	0.50	43
10%v/v 1M C_2H_6SO	0.51	42

Figure 1(a) indicates the time dependence of the open circuit potential (OCP) during the initial 6000 seconds, where the OCP values of Al in the electrolytes increased up to the 2000^{th} second, and remained relatively constant (i.e. stable) thereafter. It is observed that all the OCP curves manifest similar trends of shifting from the initial potential towards a positive value. This is the consequence of fast generation of the adsorbed intermediates (i.e. Al(OH), $Al(OH)_2$ and $Al(OH)_3$). The system at a potential below the OCP values is more thermodynamically stable (i.e. less tendency to corrosion), while the potential above the OCP, promotes corrosion. The OCP values of the 4M KOH and KOH/additives are reported in Table 2. The Na_2SO_4/KOH shows the lowest OCP value of approximately -1.57, while the highest OCP value of about -1.50 is seen for the $K_2S_2O_8$. The OCP values of Na_2SO_4, Na_2SO_3, $C_6H_5SO_2OH$ and C_2H_6SO are more negative compared to the additive-free KOH solution - indicating that the cathodic reaction is prominently retarded. The suppression of cathodic reaction leads to more negative potential owing to the accumulation of more electrons released from the anodic dissolution ($Al \rightarrow Al^{3+}$). Similarly, with the $K_2S_2O_8$ additive, a positive shift in the OCP value is observed. This is an indication of the formation of a protective layer, resulting in the suppression of the anode's corrosion. Figure 1b demonstrates the electrochemical window (EW) of various electrolytes with and without additives. EW is defined based on the highest occupied molecular orbital (HOMO) and the lowest

unoccupied molecular orbital (LUMO) as a key factor in battery's chemistry. The operating potential range of the additive/electrolyte is confined to the stability of the EW [31]. The theoretical gas evolution potentials (E_{H2}) for hydrogen evolution and the oxygen onset potential $E_{H2O/O2}$ (H_2, O_2) can be determined by the thermodynamic equations below [32]:

$$E_{H_2} = -0.059\, pH \tag{3}$$

$$E_{H_2O/O_2} = 1.23 - 0.059\, pH \tag{4}$$

The theoretical stability window of electrolyte can be calculated according to equations 3 and 4 using the pH value of the electrolyte (Table S1). The EWs of the electrolyte containing $K_2S_2O_8$, Na_2SO_4 and Na_2SO_3 are slightly increased compared to the additive-free KOH, whereas the electrolytes with $C_6H_5SO_2OH$ and C_2H_6SO specify a negligibly lower value in contrast to the 4M KOH solution. The onset potential of the oxygen evolution reaction shifts slightly towards the positive values with the inorganic additives. The results suggest that the addition of additives is not significantly effective on EW.

Potentiodynamic polarisation curves for KOH electrolyte, with and without the additives (Figure 1c), show the impact of various SO groups on the corrosion behaviour of Al in 4M KOH. The Tafel fitting was employed to calculate the corrosion current density (I_{cor}), corrosion potential (E_{cor}), cathodic Tafel constant (β_c), and the anodic Tafel constant (β_a) from the polarisation curves (Table 2). The corrosion current (I_{cor}) and corrosion potential (E_{cor}) can be obtained by Tafel extrapolation of the cathodic and anodic branches. The Tafel slope for both the cathodic and anodic reactions is described by the Butler-Volmer equation as follows [31,33]:

$$i = I_{cor}\left(e^{\frac{2.303(E-E_{cor})}{\beta\alpha}} - e^{\frac{2.303(E-E_{cor})}{\beta c}}\right) \tag{5}$$

$$\eta = \frac{-RT}{n\alpha F}\ln(i_o) + \frac{RT}{n\alpha F}\ln(i) \tag{6}$$

where $\eta=(E - E_o)$ defines the overpotential or the difference between the standard and electrode potentials. Both values of i and i_o are the current density and the exchange current density, respectively. The parameters n, α, T , R and F are the number of electron, the transfer coefficient, the absolute temperature, the universal gas constant (8.314 $Jmol^{-1}K^{-1}$) and Faraday's constant (96485 C mol^{-1}) , respectively. The exchange current density (i_o) can be determined from the plot of η vs. $\ln(i)$. The parameters i_o and α can be calculated by regression analysis. The polarization of electrode occurs when the

potential value at open circuit or corrosion potential is forced away from the rest potential. R_p, as the polarization resistance, can be determined using cathodic and anodic slopes (Stern-Geary equation) as [33]:

$$R_p = \frac{\beta_\alpha(\beta_c)}{2.303 I_{cor}(\beta_a+\beta_c)} \quad (7)$$

Table 2 Polarization parameters of the KOH electrolyte with and without the additives.

Electrolyte	E_{cor}	I_{cor}	β_a	β_c	OCP	R_P	Efficiency
unit	V	$mAcm^{-2}$			V	Ω	%
KOH	-1.350	0.025	-0.1046	-1.169	1.53	1.66	---
1.5%v/v 1M $K_2S_2O_8$	-1.364	0.016	-0.1860	0.1679	1.50	2.41	36.90
6.5%v/v 1M Na_2SO_4	1.355	0.013	-0.2142	0.176	1.57	3.32	49.88
5 %v/v 1M Na_2SO_3	-1.405	0.018	-0.2138	-0.214	1.53	2.60	29.21
6.5%v/v 1M $C_6H_5SO_2OH$	-1.371	0.011	-0.2706	0.212	1.54	2.59	45.33
16.5%v/v 1M C_2H_6SO	-1.364	0.016	-0.2045	0.152	1.53	2.38	36.90
6.5%v/v Na_2SO_4/ C_2H_6SO	-1.48	0.017	0.1217	0.121	1.55	1.48	29.20
6.5%v/v Na_2SO_4/ $C_6H_5SO_2OH$	-1.55	0.026	0.2712	0.269	1.51	2.2	-2.2

The presence of additives translates into a negative shift in the corrosion potentials, which is consistent with the results reported by Liu et al. [14] and T. Hiral et al. [34]. The cathodic branches of the polarization curves of different electrolytes containing $K_2S_2O_8$, Na_2SO_4, Na_2SO_3, $C_6H_5SO_2OH$ and C_2H_6SO are clearly lower than 4M KOH (no additive). The presence of additives has a moderate impact on the anodic branch of the curves, and no alteration is observed on the anodic dissolution of the Al electrode. The anodic and cathodic reaction of Al in the alkaline solution is described by the equations below:

Anodic reaction:

$$Al + 4OH^- \rightarrow Al(OH)_4^- + 3e^- \quad (8)$$

Cathodic reaction:

$$1/2O_2 + H_2O + 2e^- \rightarrow 2OH^- \quad (9)$$

The Al anode can deliver a higher electrochemical activity in the additive-free 4M KOH electrolyte with a higher corrosion rate than that of the KOH with additives. In spite of severe corrosion, the oxide layer (Al_2O_3) on the Al's surface is effortlessly dissolved in the alkaline solution. The presence of the additives slightly changes the

E_{cor}, I_{cor} and the inhibition efficiency. Figure S2 depicts a narrow current density scope with a moderate potential window for the $K_2S_2O_8$, $C_2H_5OHSO_2$ and C_2H_6SO in the anodic branch, implying the suppression during the anodic dissolution process by the passivation layer over the surface of the Al anode. Na_2SO_4 and Na_2SO_3 are associated with a wider current density scope for both anodic and cathodic branches. The optimal concentration of the additives was attempted to investigate the polarization curves for completed dissolution of Al anode (Figure 1d). According to Figure 1d, the dissolution of Al in the presence of the additives is higher than that using the KOH (135 min). This highlights the effectiveness of the employed additives. The Tafel slopes of the anodic curve with additives decrease compared to the KOH solution. Nevertheless, it is the opposite with the cathodic slope, which stipulates a smaller change in the current with change in the potential. The corrosion potential (E_{cor}) shifts towards negative values (Fig. 1c) for the KOH electrolyte with additives, compared to the additive-free counterparts which are consistent with the OCP results. The inhibition properties of these additives can be due to the electron pairs of the oxygen atom in the SO group; it contains a lone pair of electrons which can form a complex with the Al [35-37]. It was reported that $K_2S_2O_8$ demonstrates less discharge performance than the KOH as a result of the generation of short-lived sulphate radicals ($SO_4^{\bullet -}$) with high oxidation potentials. Sulphites, sulphates and persulphate anions are feasibly reduced to different products according to following reactions [38,39]:

$$2SO_3^{-2} + O_2 \rightarrow 2SO_4^{-2} \quad (10)$$

$$SO_4^{-2} + 9H^+ + 8e^- \rightarrow HS^- + 4H_2O \quad (11)$$

$$S_2O_8^{-2} + H_2O \rightarrow \frac{1}{2}O_2 + 2SO_4^{-2} + 2H^+ \quad (12)$$

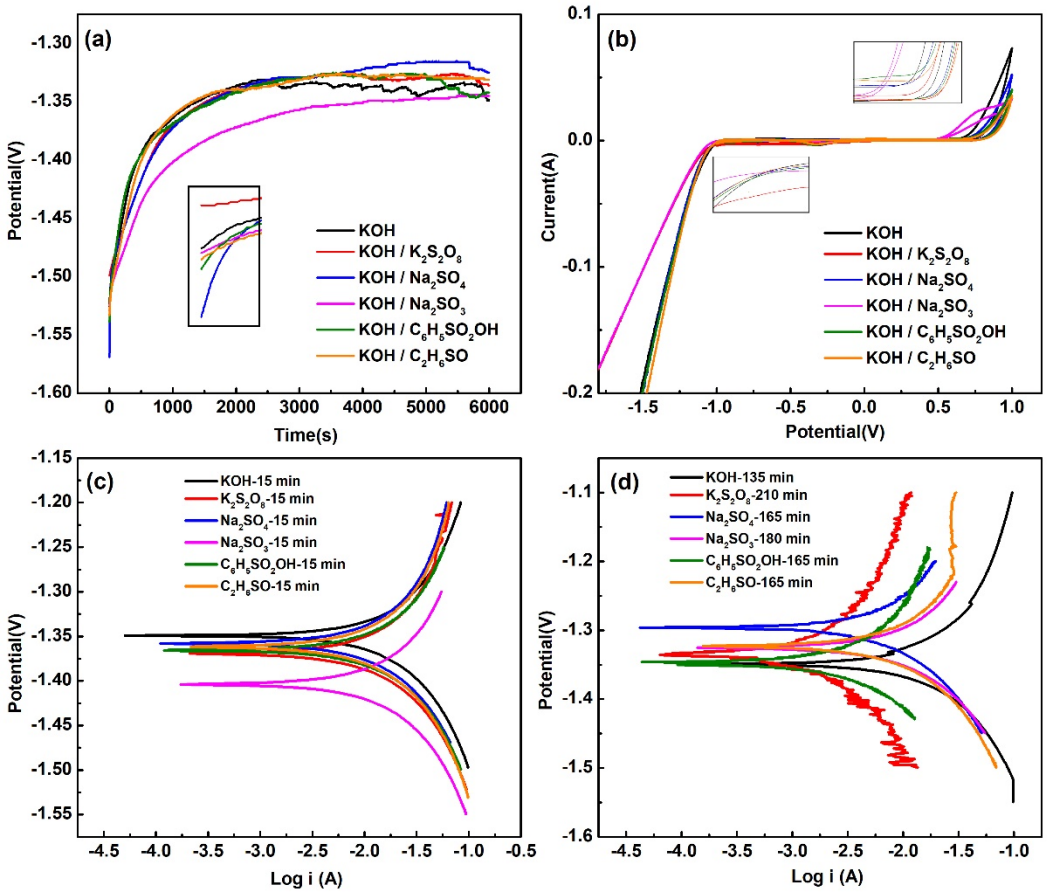

Figure 1 (a) Open circuit potential for various types of electrolytes, (b) electrochemical stability window for various types of electrolytes, (c) Tafel plots of Al in various aqueous electrolytes for 15 min of immersion time and (d) the Tafel plot of Al in terminal.

The corrosion behaviour of the species at the electrode/electrolyte interface was analysed via electrochemical impedance spectroscopy (EIS). Figure 2a displays the Nyquist plots for the Al electrode in the 4 M KOH solution with various additives. The plots exhibit non ideal semicircles (i.e. elliptic shapes) for all electrolytes with three loops at high, medium and low frequencies. The Nyquist plots were fitted with circuit elements using Ec-lab demo software in the inset of Figure 2a. The Nyquist plots are highly consistent with the experimental data, indicating a good match with the selected equivalent circuit model. Elements including, resistance (R), inductance (L) and the constant phase element (Q) are used in order to find the equivalent circuit model for the prime fitting with the experimental data. The equivalent circuit model consists of (i) a large capacitive and inductive loop at high frequency, (ii) the second capacitive loop at the medium frequency and (iii) the third capacitive loop and the second small inductive loop at low frequency. The inductive behaviour at high frequency occurs due to the intrinsic instability of the Al in the KOH solution. The first capacitive semicircle (high

frequency) is attributed to the formed passivation layer on the Al's surface due to the additives. The inductive loop is ascribed on the adsorption of Al_2O_3 and other hydroxides on the Al's surface. The second capacitive loop can be caused by the redox reaction $Al \leftrightarrow Al^+$, implicating the rate-determining step in the charge transfer process. The third capacitive semicircle is attributed to the redox reaction $Al^+ \leftrightarrow Al^{3+}$. Similar inductive loops have been observed with the adsorption of intermediate products on the Al's surface [4,13,14,40,41]. By adding additives to the electrolyte, the diameter of semicircles (charge transfer resistance) increase, owing to the passivation layer formation over the anode's surface. A strong and stable coverage of the passivation layer on the anode's surface, employing Na_2SO_4 / KOH, is observed, while $C_6H_5SO_2OH$ indicates the lowest coverage of the passivation layer on the Al's surface. The XPS analysis also confirms that the passive layer formation leads to a delay in self-corrosion in the presence of the additives. The R_1 value (the solution resistance) increases in the presence of various additives as subsiding the OH ions and conductivity.

Figure 2b displays an obvious difference in the Nyquist plots by hybridization of the two additives (i.e. inorganic Na_2SO_4 with organic $C_6H_5SO_2OH$ and C_2H_6SO), showing the significant change in the surface of the Al anode. The impedance spectra mainly consists of two semicircles, where the first capacitive semicircle at the high frequency resembles the protective film formed on the anode surface, while the second capacitive semicircle at the low frequency corresponds to the redox reactions of Al in the hybrid electrolytes. It is found that the inductive loop disappears at the medium frequency region compared to the plots shown in Figure 2a, demonstrating the formation of a protective film through the accumulation of the intermediate products which may be bonded to the Al^{3+} ions, resulting in a reduction in the $Al(OH)_4$ formation. Indeed, the hybrid composition of organic and inorganic additives hinders the self-corrosion of Al's surface, possibly as a positive synergic effect. The complex formation of the additives with the Al^{3+} ions has a negative synergic effect as a result of the consumption of the metal ions. The extracted EIS parameters of Al in the 4M KOH solution, with additives and hybrid electrolytes, are described in Table 3 and 4, respectively.

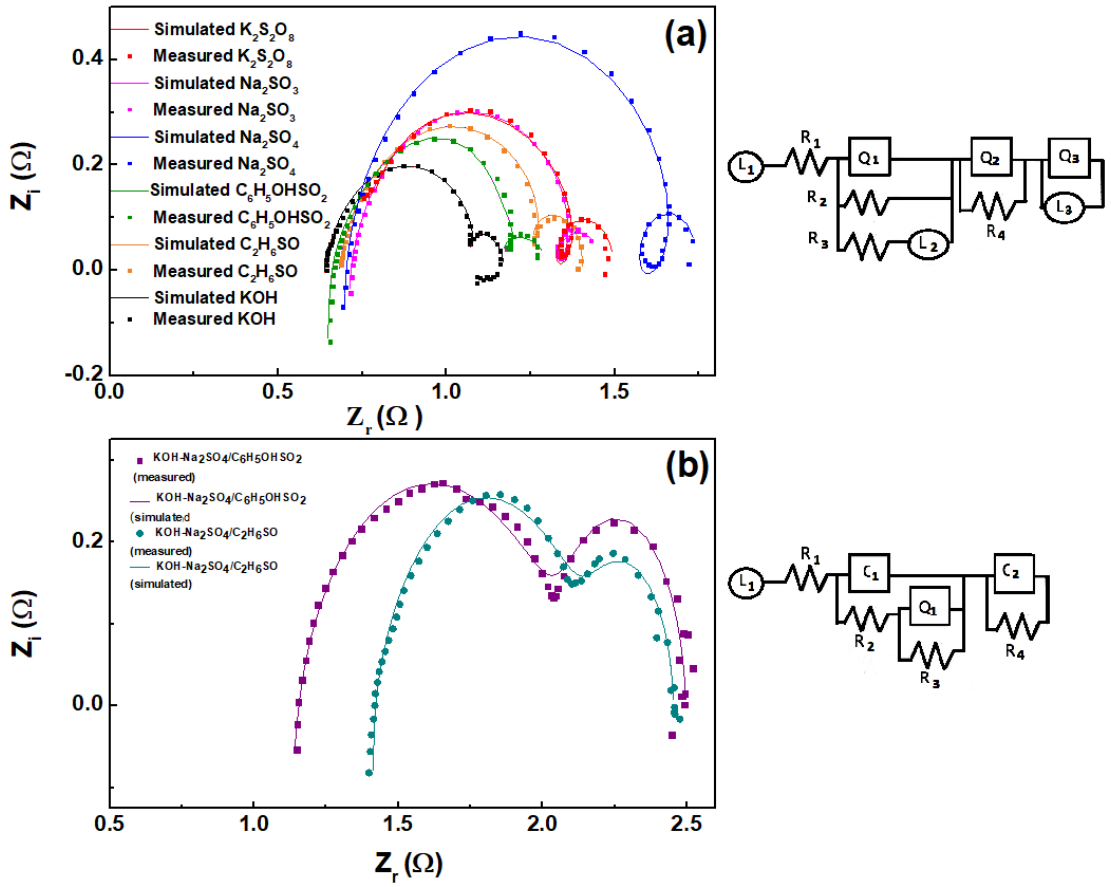

Figure 2 (a) The Nyquist plots of the Al's surface in various electrolyte and (b) the Nyquist plots of the Al's surface in the hybrid electrolytes (organic-inorganic).

Table 3: The polarization parameters of Al in 4M KOH with various additives.

	L_1	R_1	Q_1	n_1	R_2	R_3	L_2	Q_2	n_2	R_4	Q_3	n_3	L_3
Electrolyte	**H**	**Ω**	**$F.s^{(n_1-1)}$**		**Ω**	**Ω**	**H**	**$F.s^{(n_2-1)}$**		**Ω**	**$F.s^{(n_3-1)}$**		**H**
KOH	3E-08	0.39	1.7E-03	0.99	1.5	0.3	6.3E-01	1.2E-03	0.87	0.49	3.74	0.01	0.7015e-
$K_2S_2O_8$/KOH	1.89E-8	0.47	6.97E-1	0.7	1.5	10.1	9.28E-3	8.3E-02	1.1	0.15	1.88	0.0001	1.2E-05
Na_2SO_4/KOH	2E-07	0.48	1.1E-01	1.2	0.15	40.64	0.99	2.2E-04	0.89	1.1	4.67	0.83	1.9E-04
Na_2SO_3/KOH	1E-07	0.62	1.1E-01	0.97	0.18	0.8	6.2E-	3.4E-04	6.3	4.8	0.06	0.00009	9.8E-05
$C_6H_5SO_2OH$/KOH	3E-07	0.64	5.2E-03	0.72	0.96	1.17	6.5E-04	0.2557	0.75	0.14	0.93	0.51	70.83e.6
C_2H_6SO/KOH	5E-08	0.68	1.2E-03	0.85	0.68	2.5	5.1E-03	0.0205	1.11	0.19	2.32	3.91	1.2E-07

Table 4: The polarization parameters of Al in the two types of the hybrid electrolytes.

	L_1	R_1	C_1	R_2	R_3	Q_1	n_1	R_4	C_2
Hybrid Electrolytes	**H**	**Ω**	**F**	**Ω**	**Ω**	**$F.s^{(n_2-1)}$**		**Ω**	**F**
Na_2SO_4/$C_6H_5SO_2OH$-KOH	2E-07	1.071	1.78E-6	0.0289	1.015	3.07E-3	0.615	0.383	0.0339

Na_2SO_4/C_2H_6SO-KOH	2.5E-07	1.397	26.43E-12	0.006	0.7789	2.81E-3	0.725	0.273	0.042

3.2 Characterization of Anode's Surface

The SEM images of Al in the KOH electrolyte with various additives are seen in Figure 3a-3f. The pristine Al in the inset of the figures exhibits a smooth morphology without any cracks or holes on the surface. It contains a native oxide layer which can act as the nucleation or etching sites when immersed in the KOH solution, resulting in the formation of pits and cracks. The immersion of Al in a aqueous KOH solution initiates an etching process which leads to the generation of a rough porous structure on the Al's surface (Figure 3a). The deposited particles on the Al's surface could cause an interaction between the Al and the OH ions. Craterlike micro-features with grooves are clearly seen after a 30-min immersion in the 4M KOH solution. Figure 3b shows the formed micro structured pits with white precipitates when KOH/$K_2S_2O_8$ is used. A smoother surface with less corrosion pits are observed with both KOH/Na_2SO_4 and KOH/Na_2SO_3 (Figure 3c and 3d). This indicates that the adsorbed additives can inhibit the self-corrosion of the Al. The morphological features remain similar for the three additives of KOH/$K_2S_2O_8$, KOH/Na_2SO_4 and KOH/Na_2SO_3, displaying no cracks and pits on the protective layer. The electrolyte with the $C_6H_5SO_2OH$ additive (Figure 3e) shows a rough surface with large amounts of uniformly distributed pits on the corrosive Al's surface with significant deposited corrosion products. A number of cracks are visible in Figure 3f, manifesting the complex and loosen film formed by C_2H_6SO. The Al's surface in the presence of the inorganic additives is less rough than that with the organic additives - showing a stronger protective layer. It can be due to the adsorption of additives to form a protective film over the active sites for hydrogen evolution reaction, leading to a drop in the contact of the water molecules on the anode's surface. Correspondingly, the contact-angle measurements (Figure 4) show that the electrolyte with additives demonstrates less wettability compared to the 4M KOH electrolyte. On the other hand, the presence of additives corresponds to a minor corrosion degree compared to the additive-free electrolyte.

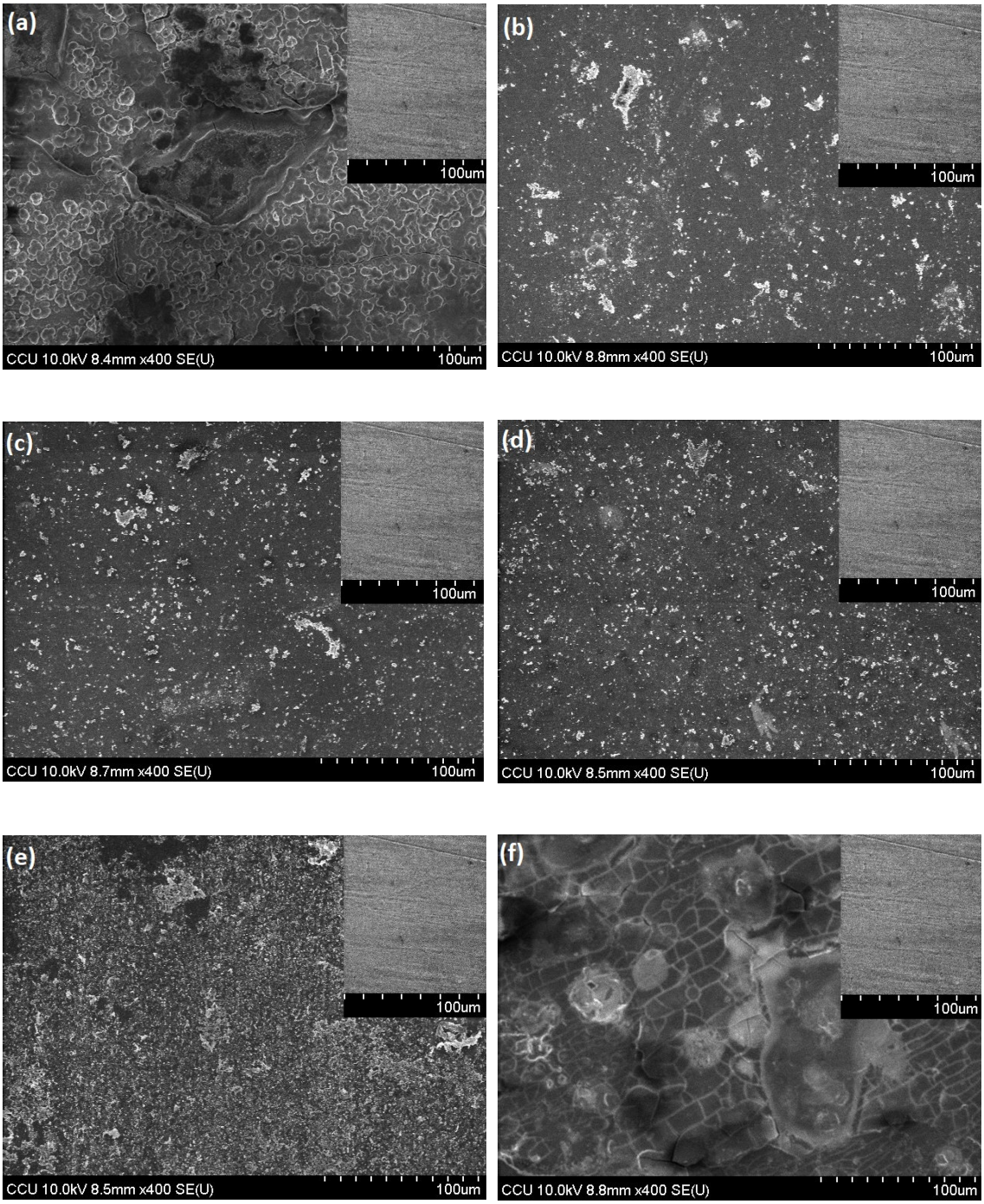

Figure 3: SEM images of the aluminium's surface after 2 hours of immersion in (a) KOH, (b) $K_2S_2O_8$/KOH, (c) Na_2SO_4/KOH, (d) Na_2SO_3/KOH, (e) $C_6H_5SO_2OH$/KOH, (f) C_2H_6SO/KOH.

The wettability of the anode-electrolyte interface was examined by measuring the contact angle of the anode's surface with different electrolytes (Figure 4). The contact angles are 26°, 55°, 65°, 54°, 52° and 53° for KOH, $K_2S_2O_8$, Na_2SO_4, Na_2SO_3, $C_6H_5SO_2OH$ and C_2H_6SO, respectively. The wettability of the additive-free KOH

solution on the Al anode is superior to the KOH solution with additive. The wettability of solution on the Al anode's surface decreases with an increase in the contact angle. This is due to the fact that fewer H_2O molecules are in contact with the Al's surface, leading the inhibition of the corrosion process and hence, a reduction in hydrogen generation. The contact angle reduces to 26° which can be related to the rougher corroded Al's surface with the 4M KOH solution. The contact angle is measured to be between 53° and 65°, indicating less wettability in the presence of different electrolytes, resulting in a reduction in self-corrosion.

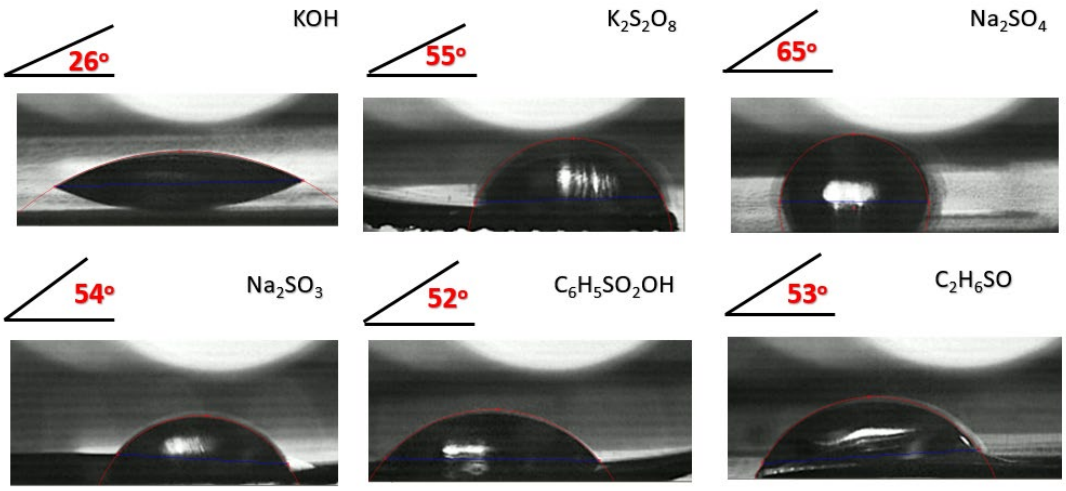

Figure 4 The contact angle between the Al anode and different electrolytes with and without the additives.

Figure 5a shows the XRD patterns of the Al's surface after 1 h of immersion in the 4M KOH solution (with an without additives). Subsequently, pure Al is examined for comparative analyses. Figure 5a reveals four diffraction peaks at 2θ values of 37.4°, 44.3°, 65.2° and 78.4°, which are highly consistent with the lattice face (311), (220), (200) and (111), and correspond to metallic aluminium [JCPDS No. 89-4037]. A weak and broad peak is easily observed at around 20°, indicating the existence of Al_2O_3 phase as the native oxide on the Al's surface (i.e. the passivation layer). A noticeable intense peak is observed at 18.1° for KOH and KOH/$K_2S_2O_8$. Similar but a less intense peak is detected with other additives. The peak corresponds to (020) as a result of the formation of AlO(OH) (aluminium oxy-hydroxide) as an intermediate species. It was reported that the intermediates (e.g. AlO(OH)) could be predicted from a mathematical model based on the critical pressure of H_2 bubbles inside the oxide's passivation layer [42]. The results indicate that the deposited layer on the surface is mostly insoluble oxide, or hydroxide, of the Al. The deposited layer, composed of sulphur and its insoluble oxide/hydroxide, may provide a fairly good protection for the Al anode by retarding the

self-corrosion process. It is observed that the peak relating to the AlO(OH) (crystal) is relatively smaller for Na_2SO_4, Na_2SO_3, $C_6H_5SO_2OH$ and C_2H_6SO. It can be concluded that the adsorbed additive molecules reduce the crystal formation on the protective layer.

Fourier transform infrared spectroscopy technique provides the information on the functional groups in the molecular structure within the range of 400 to 4000 cm^{-1}. The FT-IR spectra of the Al anode after two hours of immersion in KOH and KOH/Na_2SO_4 electrolytes are shown in Figure 5b. The wide band at 3461 cm^{-1} and 3401 cm^{-1} are attributed to the O–H stretching vibration of adsorbed water in products related to KOH and KOH/Na_2SO_4 electrolytes, respectively. There are some small absorption peaks within the range of 500–1000 cm^{-1} for the KOH electrolyte which can be attributed to the Al–O band (e.g. Al_2O_3, AlOOH) [43]. The peaks at 995 cm^{-1} is assigned to the O-H stretching of the Al-OH-Al. The sharp absorption peak at 1403 cm^{-1} can be attributed to the bridged –OH group in the corrosion product - $Al(OH)_3$. For the Al anode immersed in KOH/Na_2SO_4, the sharp peak at 609 cm^{-1} can be attributed to the SO_4^{-2} bending vibration with KOH/Na_2SO_4 electrolyte. The band at 1095 cm^{-1} corresponds to the symmetric S=O band and 1301 cm^{-1} symmetric S=O stretching vibrations in the KOH/Na_2SO_4, indicating the adsorption of the –SO groups on the Al's surface. The integration of the Al into SO_4^{-2} may be confirmed by the peak observed at 1161 cm^{-1} (Al-S) bond [44]. Na_2SO_4 molecules can be adsorbed on to the surface of the anode to make a complex interaction with Al, implying a suitable additive as corrosion protection to Al. The FTIR peaks before and after adding Na_2SO_4 to KOH solution changed due to varying in energy of the bonds within the additive molecule, owing to surface adsorption on the Al's surface. The complex film effectively suppresses the self-corrosion of Al anode in the KOH solution.

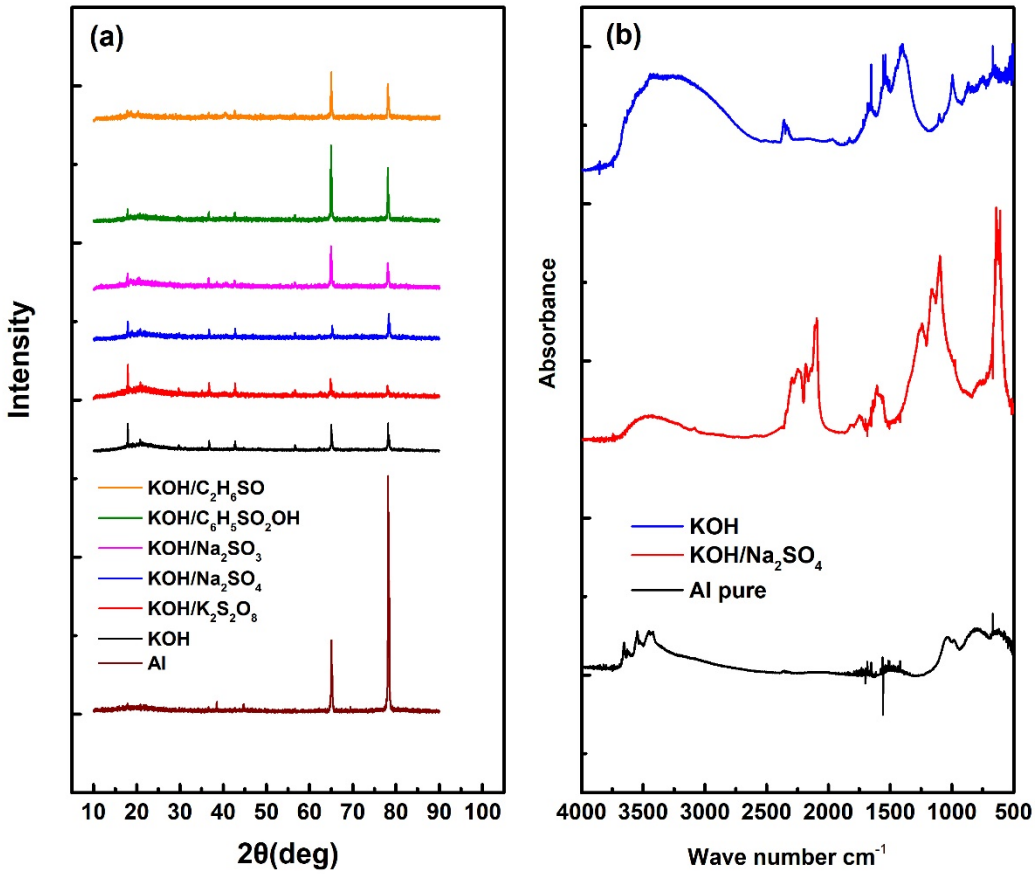

Figure 5 (a) The XRD patterns of aluminium's surface after two hours of immersion in different electrolytes, and (b) FTIR analysis of KOH and KOH/Na_2SO_4 electrolytes.

The composition of the protective layer and the surface reactions can be determined via XPS analysis. The XPS analysis was performed for Al anode after galvanostatic discharge at a current density of 10 mA cm^{-2} for 1 h. The full survey of the XPS spectra is shown in Figure S3. The peaks at the binding energies of 284.6, 74.1 and 531.1 eV correspond to C 1s, Al 2p and O 1s, respectively. The Al 2p and O 1s spectra of the Al anodes, after experiments in the KOH, Na_2SO_4/KOH and $C_6H_5SO_2OH$/KOH electrolytes, are shown in Figure 6. Deconvolution of the O 1s spectra comprises of the peaks with a small difference in the binding energy (O ls) for OH^-, H_2O and O^{-2} species. The O1s peaks can be fitted with two components at binding energies of 531 and 532.1 eV for KOH, while the O 1s spectra of the Na_2SO_4/KOH and $C_6H_5SO_2OH$/KOH consist of three oxygen species. The lower binding energy is assigned to the interaction between the metal and oxygen atom, while the higher binding energy peak is associated with the oxygen and the metal-OH bond [45]. The oxygen in the SO group is expected within the adsorbed passivation layer that is formed in the presence of the Na_2SO_4 and $C_6H_5SO_2OH$. The Al 2p spectra of the aluminium

anode reveal two peaks at 73 and 74.5 eV arising from the Al^{3+} in the oxide films of Al_2O_3 and $Al(OH)_3$, respectively. In the presence of the additives, the strength of the peak associated with $Al(OH)_3$ is significantly higher than that of the Al_2O_3 [45-47]. An extra peak is observed at the binding energy of 74.1 eV, which corresponds to the aluminium matrix (Al), suggesting that the additives are able to protect the Al's surface compared to the additive-free KOH solution. The results confirm that both additives protect the Al's surface by reducing Al_2O_3 formation and establishing a passivation layer containing oxygen bonding-based species.

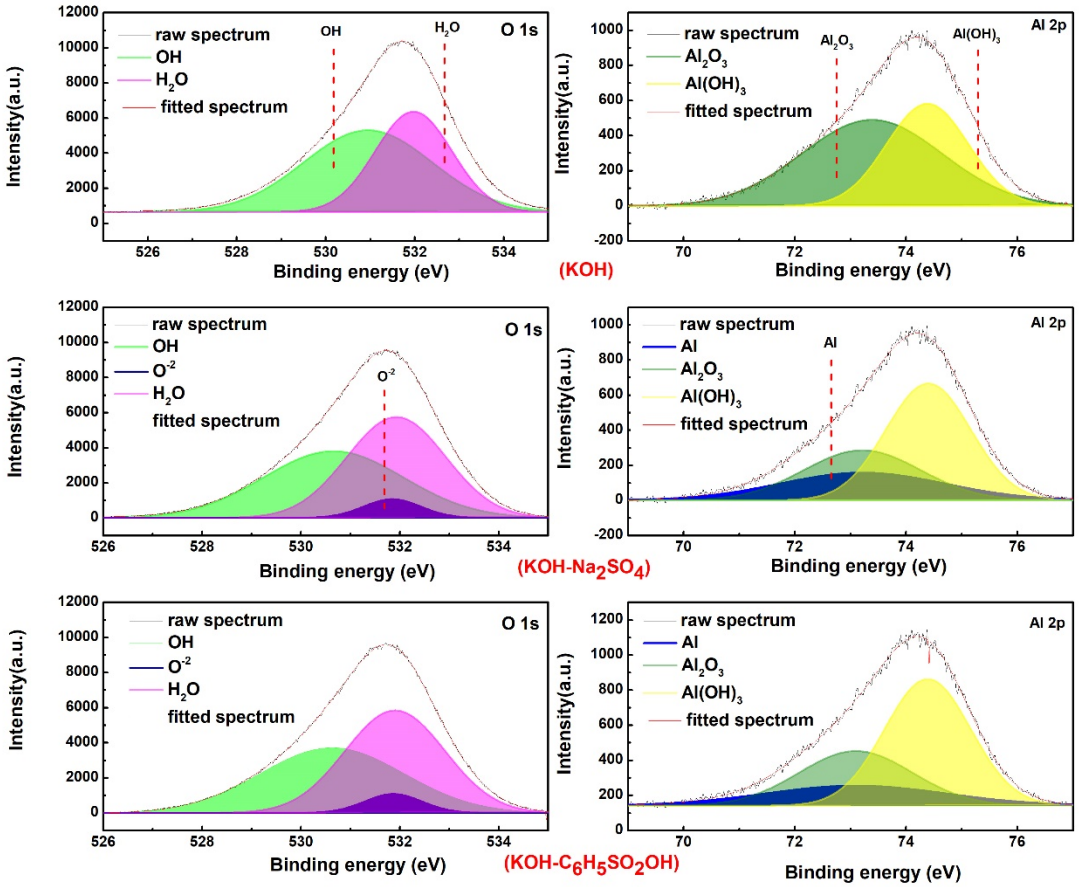

Figure 6 The XPS patterns of the Al's surface for three electrolytes (a) KOH, (b) Na_2SO_4/KOH, and (c) $C_6H_5SO_2OH$/KOH.

3.3 Mechanism of Corrosion Inhibition

The alkaline electrolyte causes the local breakdown of the passivation film (Al_2O_3) on the Al's surface, and the layer gradually disappears after being brought in contact with 4M KOH for a period of time. Anodic and cathodic reactions are expressed as described by equations 8 and 9. A Pourbaix diagram shows that Al metal can be corroded at pH values between 1 and 4, while it is passivated (immune to corrosion) in pH values of >4 and <9. Similarly, the corrosion occurs in alkaline media at pH values of 9-14 with distinct products in different zones (Figure S4a) such as Al^{3+} (acid), $Al(OH)_3$, Al_2O_3 (neutral) and $Al(OH)_4^-$ (alkaline) [48]. Several researchers have suggested that aluminium corrosion in alkaline solution can follow a two-step mechanism: (i) OH^- ions attack Al_2O_3, leading to its dissolution and resulting in $Al(OH)_3$ formation, and (ii) chemical formation of aluminate ions ($Al(OH)_4^-$). Al dissolution proceeds via the formation of hydroxide film (partial anodic reaction). This film is formed as a result of the migration of the OH^- ions through the oxide layer on the Al's surface. The reactions can be described as follows [22,2]:

(i)

$$Al_2O_3 + H_2O \leftrightarrow 2AlOOH \quad (13)$$

$$AlOOH + H_2O \leftrightarrow Al(OH)_3 \quad (14)$$

The $Al(OH)_3$ layer can be chemically dissolved in the presence of OH^- ions to form soluble aluminate ions ($Al(OH)_4^-$):

(ii)

$$Al(OH)_3 + OH^- \leftrightarrow Al(OH)_4^- \quad (15)$$

The deposited $Al(OH)_3$ can be observed around the pitted areas. Different S-O groups (SO_4-SO_4, SO_4, SO_3, SO_2 and SO) are introduced in order to retard the pitting initiation. All types of the studied additives have the potential to reduce hydrogen evaluation. Nevertheless, the electrochemical behaviour and practical battery operation are also key factors to enhance the overall performance in Al-air batteries. The surface morphologies of the samples propose that the inorganic additives are more efficient than the organic counterparts, owing to less crevice corrosion. This shows that the sulphate and sulphite anions have no adverse impacts on the passivation layer (Al_2O_3). The breakdown of the passive film on the Al's surface in alkaline/acid medium should be delayed to protect corrosion via pitting. The lowest OCP value and the highest inhibition efficiency are good evidence for the absorption effect of sulphate anions

compared to that of the sulphite anions', leading to the re-formation of a sulphate film layer on the Al's surface (Figure S4b).

The electrostatic interaction between the additive and other molecules can be mapped by employing the molecular electrostatic potential (MESP) method. The electrostatic potential of a molecule provides an electric field to study the interactions between the molecule and the other molecules through the Coulomb force. MESP map for Na_2SO_4, Na_2SO_3, $K_2S_2O_8$, C_2H_6SO and $C_6H_5SO_2OH$ compounds was calculated via DFT (B3LYP/6-31G) using Gaussian 09W A.01 package and visualized in Gaussview 6.0.16. MESP shows a 3D visual method to investigate the net electrostatic effect of the compounds and their physiochemical properties with donor electron (negative electrostatic potential) and acceptor electron (positive electrostatic potential) with an isodensity value of 0.002 a.u. Scheme 1 shows the most electrophilic regions/positive electronic potential (blue), the most nucleophilic regions/negative electrostatic capability (red), the partially negative charge region (yellow), the partially positive region (light blue), and the neutral electrostatic capability (green) identified by different color codes. The natural background was distributed around the whole molecule and the potential enhances in the order of red < orange < yellow < green < blue [49]. MESP of each component (additives of self-corrosion) is related to the charge distribution over the molecule, the polarity and dipole moment. The color code is located between -ve and +ve potential, is centred on the molecule, and provides more information on the region of electrophilic and nucleophilic attacks. A significant distinction was observed between the potential values of the organic and inorganic compounds. The minimal and maximal values are for C_2H_6SO (-0.06443 a.u. to +0.06443 a.u.) and Na_2SO_4 (-0.161 a.u. to +0.161 a.u.), respectively. The deep dark blue region in both edges of Na_2SO_4, Na_2SO_3, $K_2S_2O_8$ represents the electrophilic nature of Na or K. The main area of the molecules are seen in yellow (partially negative), whereas C_2H_6SO shows a red color for free electrons oxygen (SO) with the majority being partially positive (light blue). $C_6H_5SO_2OH$, as the other organic additive, demonstrates the fact that the majority of regions are blue or light blue, owing to electron deficiency. The electron-rich areas are more suitable for adsorption on the Al's surface, and inorganic additives provide more negative regions. The binding of additives to the aluminium's surface largely depends on the variation in electrostatic potential generated by an additive to the binding site.

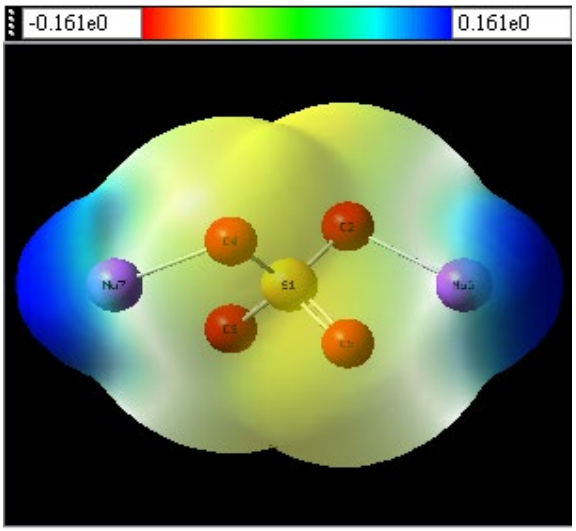

Na_2SO_4

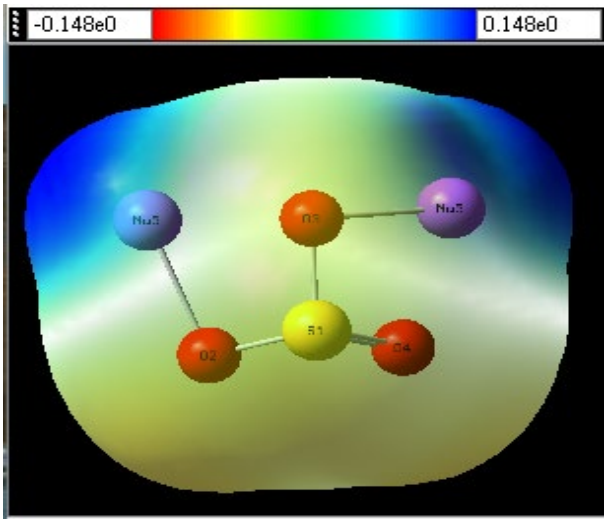

Na_2SO_3

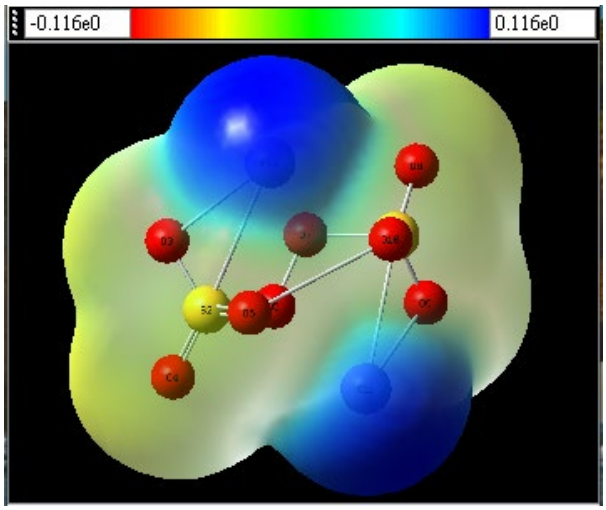

$K_2S_2O_8$

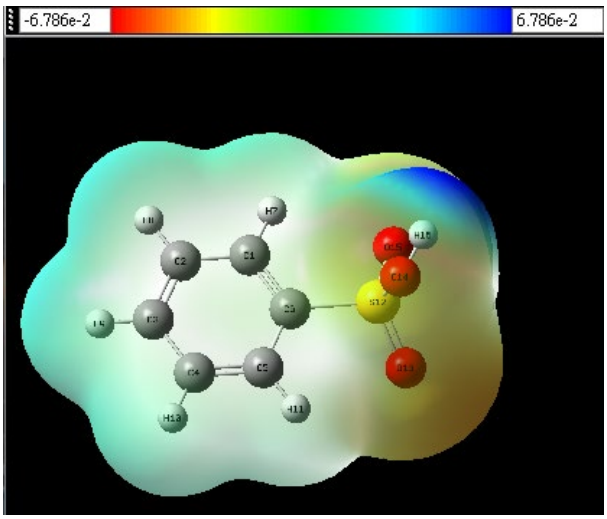

$C_6H_5SO_2OH$

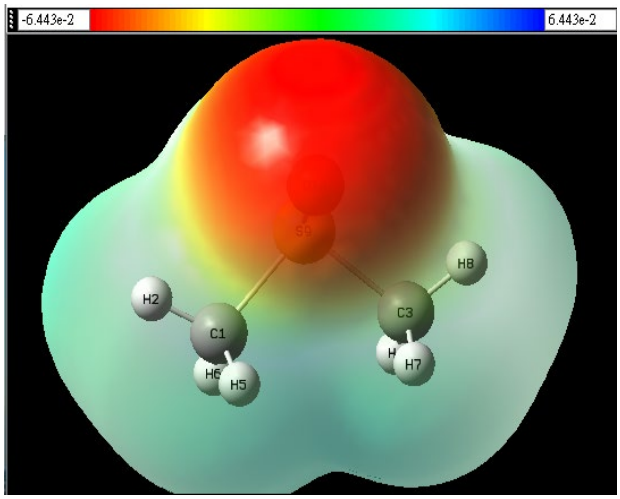

C_2H_6SO

Scheme 1 Molecular Electrostatic Potential (MEP) obtained through DFT analysis using Gaussian-09 software for the organic and inorganic additives.

3.4 Performance of the Al-Air Battery

To explore practical application, an in-house cell was fabricated based on Co_3O_4/NC-CNT air cathode [29]. The power density and polarization curves are shown in Figure 7(a). The maximum power density based on the Na_2SO_4/KOH electrolyte is measured to be 94 mWcm $^{-2}$ at a current density of 217 mAcm $^{-2}$ which is much higher than the KOH 4M solution (i.e. 60 mWcm $^{-2}$) at a current density of 150 mAcm^{-2}. It is clearly seen that the potential declines with an increase in current density as governed by the electrochemical polarization effect. All electrolytes containing additives demonstrate less voltage drop than the 4M KOH. This can be due to the less pronounced corrosion effect towards the anode electrode. An Al-air battery was assembled to evaluate the discharge performance of the additives at a constant current density of 10 mA cm^{-2}. The discharge performance of Al-air batteries typically depends on several parameters such as the anode type, ORR/OER efficiencies (air cathode) and hydrogen evolution/corrosion (electrolyte). The accumulation of intermediate products ($Al(OH)_{1ads}$, $Al(OH)_{2ads}$, $Al(OH)_{3ads}$) on the anode's surface unavoidably decreases the discharge performance leading to an obstruction to the migration of the OH^- ions. To examine the discharge performance, the influence of the additives on the self-corrosion of the Al anode was tested using the galvanostatic technique. The decline in the cell potential during the initial discharge period is related to the internal resistance of the Al-air battery. All electrolytes exhibit similar trends during the discharge process. A drop in the potential during the final stage of the discharging process is observed after the complete dissolution of the Al anode. The Al-air batteries with and without additives display stable potential of ~1.52 V, 1.43V, 1.50V, 1.54V, 1.45V and 1.37V at a current density of 10 mA cm $^{-2}$ for KOH, $K_2S_2O_8$, Na_2SO_4, Na_2SO_3, $C_6H_5SO_2OH$ and C_2H_6SO, respectively. The plateaued potentials of the Al-air batteries with the two additives of $K_2S_2O_8$ and C_2H_6SO, are lower than that of the 4M KOH's, indicating an adverse impact on the discharge potential due to rapid dissolution of the native passive layer (Al_2O_3). Figure 7b shows the improvement of the discharge capacities with the addition of Na_2SO_4, Na_2SO_3, $C_6H_5SO_2OH$ and C_2H_6SO to the electrolyte, compared to additive-free KOH solution. However, $K_2S_2O_8$ /KOH causes a decrease in the discharge capacity. The reducing effect of the peroxydisulphate $S_2O_8^{2-}$ ions in the KOH solution leads to the generation of the $SO_4^{\bullet-}$ species as a strong oxidizing radical anion. This, in turn, results in the extraction of electrons from the valence band [50,51]. The increase in the discharge capacity can be assigned to more negative potentials of the Al's anode in the

electrolyte/additives, as reported in Tafel plots (Figure 2(c)). On the other hand, the additives may prevent the accumulation of intermediate products on the Al anode's surface, the complex formation (Al^{3+} ions/additives), and reduce of evaluated hydrogen gas. The discharge capacity increases by 29%, 18 %, 1.3% and 16% in the presence of Na_2SO_4, Na_2SO_3, $C_6H_5SO_2OH$ and C_2H_6SO, respectively. The Al-air battery with the Na_2SO_4 additive achieves the highest specific capacity of 2604 $mAhg^{-1}$ (based on the mass of the Al consumed) in comparison with the capacity achieved by using the additive-free electrolyte (2021 $mAhg^{-1}$). This is associated with the noticeable increase in the anode utilization from 67.18% to 87.37%. Figure 7(c) exhibits the effect of hybrid organic and inorganic additives on the Al-air battery's performance. Na_2SO_4 as an inorganic additive was added to the organic additives $C_6H_5SO_2OH$ and C_2H_6SO to prepare hybrid electrolytes. The discharge performance of $Na_2SO_4/C_6H_5SO_2OH$ and Na_2SO_4/C_2H_6SO electrolytes are less than the discharge performance of Na_2SO_4. The discharge performance of the hybrid $Na_2SO_4/C_6H_5SO_2OH$ is also less than that of the 4M KOH's. The results suggest that there is little synergic effect for the hybrids of the studied organic-inorganic electrolyte additives. Simultaneously, the interaction of inhibitors (S), A and B, can be estimated as [52]:

$$S = \frac{(1-\eta_A-\eta_B-(\eta_A\eta_B))}{(1-\eta_{AB})} \tag{16}$$

where η_A, η_B and η_{AB} are the inhibition efficiencies of compounds A, B and AB, respectively. Typically, good performance can be achieved when the synergistic parameter is greater than the unity. The S values are found to be 0.178 and 0.073 for $Na_2SO_4/C_6H_5SO_2OH$ and Na_2SO_4/C_2H_6SO, suggesting no synergistic effect in corrosion prevention for the Al in the alkaline solution. Although, Na_2SO_4/C_2H_6SO demonstrates an inhibition efficiency of 29.20 %, this value is smaller than the individual additives of Na_2SO_4 (i.e. 49.88%) and C_2H_6SO (i.e. 36.90%).

The Al-air battery assembled with Co_3O_4/NC-CNT catalyst shows an average discharge potential of 1.2 V and an average charge potential of 2.05 V during cycling process during the discharging phase for 10 min, and charging phase for 20 min, at a current density of 10 $mAcm^{-2}$, respectively. The charge and discharge cycling processes for the electrolytes with additive-free KOH, Na_2SO_4/KOH and $C_6H_5SO_2OH$/KOH are depicted in Figure 7(d). The charge/discharge cycle performance of the Al–air batteries after the modification of the electrolyte with additives is improved. Na_2SO_4-based electrolyte exhibits a better stability and a longer cycle life with the charge and discharge potentials of 2.05 V and 1.35 V at a voltage gap of 0.7 V, as shown in Figure 7(d). The batteries using additive-free KOH exhibit a lower discharge potential (1. 13

V), indicating a higher rate of Al dissolution in the absence of a protective layer, whereas with a protective layer (with $C_6H_5SO_2OH$) a higher discharge potential (1.2 V) is recorded. The results show that these additives increase the inhibition efficiency via absorption on the Al's surface through the oxygen atoms, as well as electrons in the aromatic ring (organic additive).

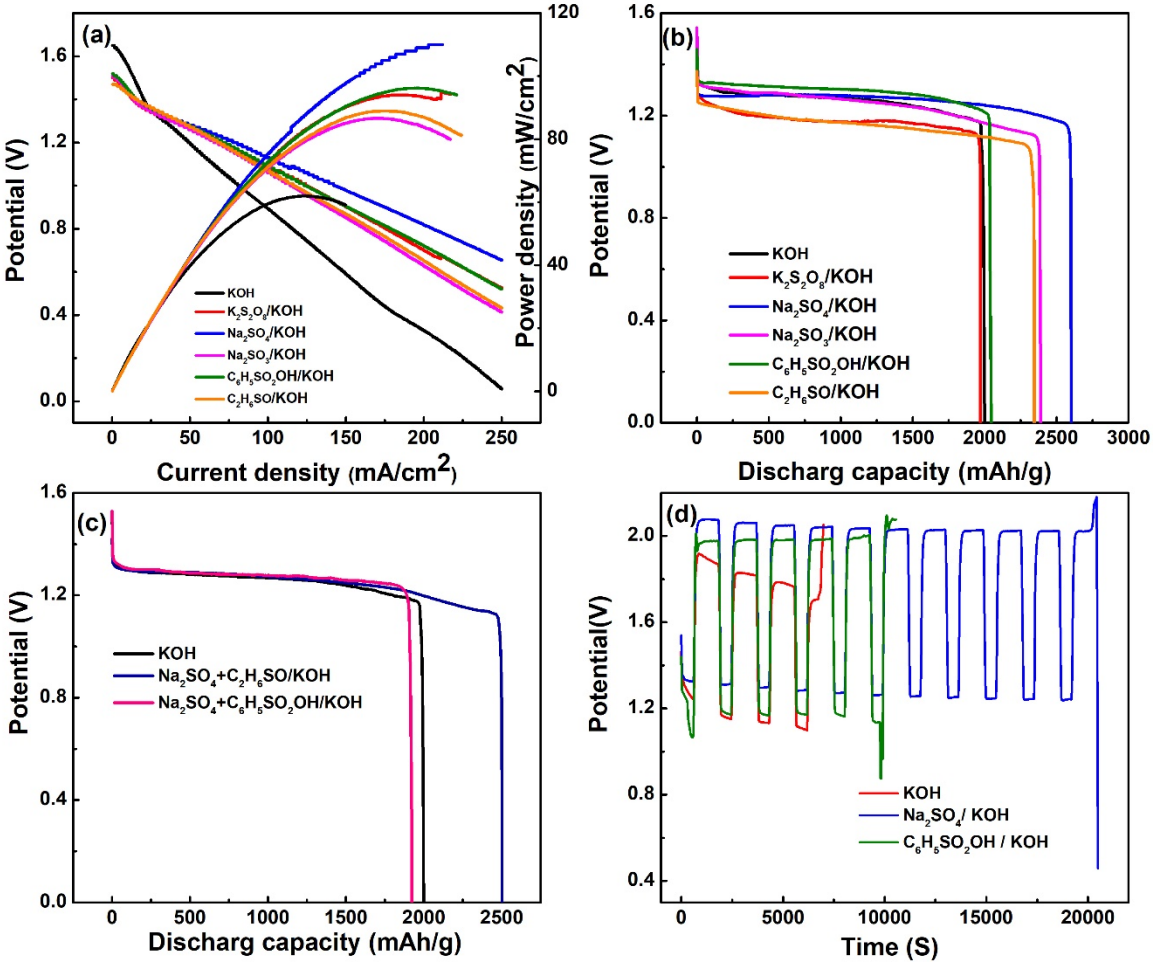

Figure 7(a) Polarization and power density curves of the Al-air batteries with various electrolytes; (b) a galvanostatic discharge curves of Al–air batteries with different electrolytes at a current density of 10 $mAcm^{-2}$, (c) a galvanostatic discharge curves of Al–air batteries with hybrid of organic and inorganic electrolytes, and (d) charge/discharge cycling performance of the three electrolytes at a discharge current density of 10 $mAcm^{-2}$ for 10 min and a charge current density of 20 $mAcm^{-2}$ for 20 min.

4. Conclusion

In this study, we investigated the self-corrosion and hydrogen evolution of the Al anode in an alkaline (KOH) electrolyte in the presence of different additives, containing SO group as the inhibitor. The tests revealed that all the studies additives had the capability of diminishing hydrogen evaluation on the Al anode's surface. The electrochemical characterization showed that the investigated additives can help to slow down the unfavourable self-corrosion process. The surface morphologies of the Al anode suggest that the inorganic additives studied in this work are more effective than the organic counterparts, as a result of less pitting and fewer observed holes and cracks. Eventually, the addition of Na_2SO_4 improved the discharge performance as well as anode utilization (87.37%) in the Al-air battery due to the presence of stable SO groups and the formation of $Al_2(SO_4)_3$ as a soluble salt in the aqueous alkaline solution. The calculated synergic parameters revealed that the hybrids of Na_2SO_4 with the two organic additives of $C_6H_5SO_2OH$ and C_2H_6SO was not effective. However, both the Na_2SO_4 and $C_6H_5SO_2OH$ additives exhibited stable discharge/charge cycles in comparison with the additive-free KOH solution (at a constant voltage gap). The reduction/oxidation of SO groups in the cathode may generate different products and thus, leads to a decrease in the battery's performance. Anion-competitive adsorption on the Al's surface depends on the corresponding stability. This approach proved that the additives with stable SO groups are capable of improving the discharge performance and cyclability of the Al's surface in a rechargeable Al-air battery.

Acknowledgements

The authors would like to thank the Ministry of Science and Technology, Taiwan, for supporting this research under the MOST 108-2221-E-194-039 grant, and the Advanced Institute of Manufacturing with High-tech Innovations (AIM-HI) from The Featured Areas Research Centre Program within the framework of the Higher Education Sprout Project by the Ministry of Education (MOE) in Taiwan.

References

[1] Elia, G. A., Marquardt, K., Hoeppner, K., Fantini, S., Lin, R., Knipping, E., ... & Hahn, R. (2016). An overview and future perspectives of aluminum batteries. Advanced Materials, 28(35), 7564-7579.

[2] Wu, S., Zhang, Q., Ma, J., Sun, D., Tang, Y., & Wang, H. (2020). Interfacial design of Al electrode for efficient aluminum-air batteries: issues and advances. Materials Today Energy, 18, 100499.

[3] Durmus, Y. E., Zhang, H., Baakes, F., Desmaizieres, G., Hayun, H., Yang, L., ... & Passerini, S. (2020). Side by Side Battery Technologies with Lithium-Ion Based Batteries. Advanced Energy Materials, 2000089.

[4] Yang, H., Li, X., Wang, Y., Gao, L., Li, J., Zhang, D., & Lin, T. (2020). Excellent performance of aluminium anode based on dithiothreitol additives for alkaline aluminium/air batteries. Journal of Power Sources, 452, 227785.
[5] Craig, B., Schoetz, T., Cruden, A., & de Leon, C. P. (2020). Review of current progress in non-aqueous aluminium batteries. Renewable and Sustainable Energy Reviews, 133, 110100.
[6] Sovizi, M. R., Afshari, M., Jafarzadeh, K., & Neshati, J. (2017). Electrochemical and microstructural investigations on an as-cast and solution-annealed Al–Mg–Sn–Ga alloy as anode material in sodium chloride solution. Ionics, 23(11), 3073-3084.
[7] Sovizi, M. R., & Afshari, M. (2019). Effect of nano zirconia on electrochemical performance, corrosion behavior and microstructure of Al-Mg-Sn-Ga anode for aluminum batteries. Journal of Alloys and Compounds, 792, 1088-1094.
[8] Zhang, P., Liu, X., Xue, J., & Jiang, K. (2020). The role of microstructural evolution in improving energy conversion of Al-based anodes for metal-air batteries. Journal of Power Sources, 451, 227806.
[9] Jiang, M., Fu, C., Cheng, R., Liu, T., Guo, M., Meng, P., ... & Sun, B. (2020). Interface Engineering of Co3Fe7-Fe3C Heterostructure as an Efficient Oxygen Reduction Reaction Electrocatalyst for Aluminum–air Batteries. Chemical Engineering Journal, 127124.
[10] Jiang, M., Yang, J., Ju, J., Zhang, W., He, L., Zhang, J., ... & Sun, B. (2020). Space-confined synthesis of CoNi nanoalloy in N-doped porous carbon frameworks as efficient oxygen reduction catalyst for neutral and alkaline aluminum-air batteries. Energy Storage Materials, 27, 96-108.
[11] Lai, Y., Wang, Q., Wang, M., Li, J., Fang, J., & Zhang, Z. (2017). Facile synthesis of mesoporous Fe-NC electrocatalyst for high performance alkaline aluminum-air battery. Journal of Electroanalytical Chemistry, 801, 72-76.
[12] Yang, L., Wu, Y., Chen, S., Xiao, Y., Chen, S., Zheng, P., ... & Qu, J. E. A promising hybrid additive for enhancing the performance of alkaline aluminum-air batteries. Materials Chemistry and Physics, 257, 123787.
[13] Liu, J., Wang, D., Zhang, D., Gao, L., & Lin, T. (2016). Synergistic effects of carboxymethyl cellulose and ZnO as alkaline electrolyte additives for aluminium anodes with a view towards Al-air batteries. Journal of Power Sources, 335, 1-11.
[14] Liu, Y., Zhang, H., Liu, Y., Li, J., & Li, W. (2019). Inhibitive effect of quaternary ammonium-type surfactants on the self-corrosion of the anode in alkaline aluminium-air battery. Journal of Power Sources, 434, 226723.
[15] Deyab, M. A. (2017). 1-Allyl-3-methylimidazolium bis (trifluoromethylsulfonyl) imide as an effective organic additive in aluminum-air battery. Electrochimica Acta, 244, 178-183.

[16] Wu, S., Zhang, Q., Sun, D., Luan, J., Shi, H., Hu, S., ... & Wang, H. (2020). Understanding the synergistic effect of alkyl polyglucoside and potassium stannate as advanced hybrid corrosion inhibitor for alkaline aluminum-air battery. Chemical Engineering Journal, 383, 123162.
[17] Benchakar, M., Naejus, R., Damas, C., & Santos-Pena, J. (2020). Exploring the use of EMImFSI ionic liquid as additive or co-solvent for room temperature sodium ion battery electrolytes. Electrochimica Acta, 330, 135193.

[18]Chatterjee, K., Pathak, A. D., Lakma, A., Sharma, C. S., Sahu, K. K., & Singh, A. K. (2020). Synthesis, characterization and application of a non-flammable dicationic ionic liquid in lithium-ion battery as electrolyte additive. Scientific reports, 10(1), 1-12.

[19] Lukatskaya, M. R., Feldblyum, J. I., Mackanic, D. G., Lissel, F., Michels, D. L., Cui, Y., & Bao, Z. (2018). Concentrated mixed cation acetate "water-in-salt" solutions as green and low-cost high voltage electrolytes for aqueous batteries. Energy & Environmental Science, 11(10), 2876-2883.

[20] Jiang, H., Yu, S., Li, W., Yang, Y., Yang, L., & Zhang, Z. (2020). Inhibition effect and mechanism of inorganic-organic hybrid additives on three-dimension porous aluminum foam in alkaline Al-air battery. Journal of Power Sources, 448, 227460.
[21] Kang, Q. X., Wang, Y., & Zhang, X. Y. (2019). Experimental and theoretical investigation on calcium oxide and L-aspartic as an effective hybrid inhibitor for aluminum-air batteries. Journal of Alloys and Compounds, 774, 1069-1080.
[22]Goel, P., Dobhal, D., & Sharma, R. C. (2020). Aluminum–air batteries: A viability review. Journal of Energy Storage, 28, 101287.
[23] Namieśnik, J., & Rabajczyk, A. (2010). The speciation and physico-chemical forms of metals in surface waters and sediments. Chemical Speciation & Bioavailability, 22(1), 1-24.
[24] Quartarone, G., Bonaldo, L., & Tortato, C. (2006). Inhibitive action of indole-5-carboxylic acid towards corrosion of mild steel in deaerated 0.5 M sulfuric acid solutions. Applied surface science, 252(23), 8251-8257.
[25] Al Zoubi, W., & Ko, Y. G. (2018). Enhanced corrosion protection performance by organic-inorganic materials containing thiocarbonyl compounds. Scientific reports, 8(1), 1-11.
[26] Nie, Y., Gao, J., Wang, E., Jiang, L., An, L., & Wang, X. (2017). An effective hybrid organic/inorganic inhibitor for alkaline aluminum-air fuel cells. Electrochimica Acta, 248, 478-485.

[27] Zuo, Y., Yu, Y., Liu, H., Gu, Z., Cao, Q., & Zuo, C. (2020). Electrospun Al2O3 Film as Inhibiting Corrosion Interlayer of Anode for Solid Aluminum–Air Batteries. Batteries, 6(1), 19.
[28] Hosseini, S., Soltani, S. M., & Li, Y. Y. (2020). Current status and technical challenges of electrolytes in zinc–air batteries: An in-depth Review. Chemical Engineering Journal, 127241.
[29] Wang, C. C., Hung, K. Y., Ko, T. E., Hosseini, S., & Li, Y. Y. (2020). Carbon-nanotube-grafted and nano-Co3O4-doped porous carbon derived from metal-organic framework as an excellent bifunctional catalyst for zinc–air battery. Journal of Power Sources, 452, 227841.
[30] Zhou, C., Bhonge, K., & Cho, K. T. (2020). Analysis of the effect of hydrogen-evolving side reaction in the aqueous aluminum-air battery. Electrochimica Acta, 330, 135290..
[31] Hosseini, S., Abbasi, A., Uginet, L. O., Haustraete, N., Praserthdam, S., Yonezawa, T., & Kheawhom, S. (2019). The influence of dimethyl sulfoxide as electrolyte additive on anodic dissolution of alkaline zinc-air flow battery. Scientific reports, 9(1), 1-12.
[32] Ishaque, M., Shah, A., Iftikhar, F. J., & Akbar, M. (2020). Development of transition metal based electrolyzer for efficient oxygen evolution reaction. Journal of Renewable and Sustainable Energy, 12(2), 024102.
[33] Shinagawa, T., Garcia-Esparza, A. T., & Takanabe, K. (2015). Insight on Tafel slopes from a microkinetic analysis of aqueous electrocatalysis for energy conversion. Scientific reports, 5, 13801.
[34] Hirai, T., Yamaki, J., Okada, T., & Yamaji, A. (1985). Inhibiting effects of Al corrosion by polymer ammonium chlorides in alkaline electrolyte. Electrochimica Acta, 30(1), 61-67.
[35] Ehteshamzadeh, M., Jafari, A.H., Naderi, E. & Hosseini, M.G.(2009). Effect of carbon steel microstructures and molecular structure of two new Schiff base compounds on inhibition performance in 1 M HCl solution by EIS. Materials Chemistry and Physics, 115, 986–993.
[36] Li, X., Deng, S., & Xie, X. (2014). Experimental and theoretical study on corrosion inhibition of oxime compounds for aluminium in HCl solution. Corrosion Science, 81, 162-175.
[37] Khaled, K. F., & Al-Qahtani, M. M. (2009). The inhibitive effect of some tetrazole derivatives towards Al corrosion in acid solution: Chemical, electrochemical and theoretical studies. Materials Chemistry and Physics, 113(1), 150-158.
[38] JR Postgate. (1979). The sulphate-reducing bacteria. CUP Archive.
[39] Liu, H., Bruton, T. A., Li, W., Buren, J. V., Prasse, C., Doyle, F. M., & Sedlak, D. L. (2016). Oxidation of benzene by persulfate in the presence of Fe (III)-and Mn (IV)-

containing oxides: stoichiometric efficiency and transformation products. Environmental science & technology, 50(2), 890-898.
[40] Wysocka, J., Cieslik, M., Krakowiak, S., & Ryl, J. (2018). Carboxylic acids as efficient corrosion inhibitors of aluminium alloys in alkaline media. Electrochimica Acta, 289, 175-192.
[41] Hosseini, S., Lao-Atiman, W., Han, S. J., Arpornwichanop, A., Yonezawa, T., & Kheawhom, S. (2018). Discharge performance of zinc-air flow batteries under the effects of sodium dodecyl sulfate and pluronic F-127. Scientific reports, 8(1), 1-13.
[42] Deng, Z. Y., Ferreira, J. M., Tanaka, Y., & Ye, J. (2007). Physicochemical mechanism for the continuous reaction of γ-Al2O3-modified aluminum powder with water. Journal of the American Ceramic Society, 90(5), 1521-1526.
[43] Liu, C., Shih, K., Gao, Y., Li, F., & Wei, L. (2012). Dechlorinating transformation of propachlor through nucleophilic substitution by dithionite on the surface of alumina. Journal of soils and sediments, 12(5), 724-733.
[44] Coates, J. (2006). Interpretation of infrared spectra, a practical approach. Encyclopedia of analytical chemistry: applications, theory and instrumentation.
[45] Raju, V., Rani, J. V., & Basak, P. (2020). Self-arranged polythiophene on multi-walled carbon nanotube templated composites: Synthesis and application in rechargeable aluminium battery. Electrochimica Acta, 361, 137097
[46] Li, S. Y., & Church, B. C. (2016). Effect of aqueous-based cathode slurry pH and immersion time on corrosion of aluminum current collector in lithium-ion batteries. Materials and Corrosion, 67(9), 978-987.
[47] Ryl, J., Brodowski, M., Kowalski, M., Lipinska, W., Niedzialkowski, P., & Wysocka, J. (2019). Corrosion inhibition mechanism and efficiency differentiation of dihydroxybenzene isomers towards aluminum alloy 5754 in alkaline media. Materials, 12(19), 3067.
[48] Pourbaix, M. (1974). Atlas of electrochemical equilibria in aqueous solution. NACE, 307.

[49] da Cunha Xavier, J., Almeida-Neto, F. W. Q., da Silva, P. T., de Sousa, A. P., Marinho, E. S., Marinho, M. M., ... & Nogueira, C. E. S. (2020). Structural characterization, DFT calculations, ADMET studies, antibiotic potentiating activity, evaluation of efflux pump inhibition and molecular docking of chalcone (E)-1-(2-hydroxy-3, 4, 6-trimethoxyphenyl)-3-(4-methoxyphenyl) prop-2-en-1-one. Journal of Molecular Structure, 129692.

[50] Weyher, J. L., Tichelaar, F. D., Van Dorp, D. H., Kelly, J. J., & Khachapuridze, A. (2010). The K2S2O8–KOH photoetching system for GaN. Journal of Crystal Growth, 312(18), 2607-2610.
[51] Khezri, R., Hosseini, S., Lahiri, A., Motlagh, S. R., Nguyen, M. T., Yonezawa, T., & Kheawhom, S. (2020). Enhanced Cycling Performance of Rechargeable Zinc–Air Flow Batteries Using Potassium Persulfate as Electrolyte Additive. International journal of molecular sciences, 21(19), 7303.
[52] Murakawa, T., Nagaura, S., & Hackerman, N. (1967). Coverage of iron surface by organic compounds and anions in acid solutions. Corrosion Science, 7(2), 79-89.